Available online at www.sciencedirect.com
SCIENCE DIRECT®
ELSEVIER
International Journal of Solids and Structures 43 (2006) 3124–3141
INTERNATIONAL JOURNAL OF SOLIDS and STRUCTURES
www.elsevier.com/locate/ijsolstr

Delamination threshold load for dynamic impact on plates

Robin Olsson *, Mauricio V. Donadon, Brian G. Falzon

Department of Aeronautics, Imperial College, London SW7 2AZ, United Kingdom

Received 8 February 2005; received in revised form 5 May 2005
Available online 1 July 2005

Abstract

A criterion is derived for delamination onset in transversely isotropic laminated plates under small mass, high velocity impact. The resulting delamination threshold load is about 21% higher than the corresponding quasi-static threshold load. A closed form approximation for the peak impact load is then used to predict the delamination threshold velocity. The theory is validated for a range of test cases by comparison with 3D finite element simulation using LS-DYNA and a newly developed interface element to model delamination onset and growth. The predicted delamination threshold loads and velocities are in very good agreement with the finite element simulations. Good agreement is also shown in a comparison with published experimental results. In contrast to quasi-static impacts, delamination growth occurs under a rapidly decreasing load. Inclusion of finite thickness effects and a proper description of the contact stiffness are found to be vital for accurate prediction of the delamination threshold velocity.

Keywords: Composite materials; Delamination; Dynamic; Impact; Plate

1. Introduction

Impact damage is a major issue in the design of laminated composite structures, as it may reduce strength and stiffness significantly without any visible damage at the surface (Abrate, 1991; Davies and Olsson, 2004). The sequence of damage formation in laminated fibre composites normally involves initial matrix cracks, followed by delaminations and eventually fibre fracture. Delaminations are particularly serious since they are formed at relatively low loads and have a major influence on flexural stiffness and buckling failure.

In the aircraft industry it is customary to quantify impact threats in terms of impact energy. However, it has been demonstrated experimentally that small mass and large mass impactors of equal impact energy

* Corresponding author. Tel.: +44 20 7594 5086; fax: +44 20 7594 5078.
E-mail address: r.olsson@imperial.ac.uk (R. Olsson).

0020-7683/$ - see front matter © 2005 Elsevier Ltd. All rights reserved.
doi:10.1016/j.ijsolstr.2005.05.005

cause entirely different response and damage when impacting a plate (Olsson, 2000). It is common to classify impact as "high velocity" and "low velocity", but there is considerable disagreement on the definition of these categories. Some authors refer, improperly, to the response type under small mass impact as "high velocity" impact and under large mass impact as "low velocity" impact, but it has been shown that the response type under elastic conditions, i.e., prior to damage onset, only depends on the impactor/plate mass ratio (Olsson, 2000). The distinction between "high velocity" and "low velocity" impact may, however, be relevant when considering damage initiation, as high impact velocities are required to cause damage during a small mass impact.

Different response types are illustrated in Fig. 1. For very light impactors the impacted plate will not have time to deflect and the response will be dominated by through-thickness waves (Fig. 1a). Most small mass impactors, e.g., runway debris and hail, result in intermediate impact times where the response involves transient shear waves and flexural waves (Fig. 1b). Large mass impactors like dropped tools cause a quasi-static response, where the deflection shape and amplitude is equivalent to a static loading case (Fig. 1c). For sufficiently high velocities (usually more than 70 m/s for carbon/epoxy laminates) the impactor/plate mass ratio is irrelevant for the response type, as penetration occurs prior to any deflection.

The impact on plates involves an interaction between plate deflection and indentation. Elastic indentation of monolithic plates by hemispherical objects is commonly described by a Hertzian contact law, which assumes an infinite thickness and negligible surface curvature. The general problem of a hemispherical body impacting an orthotropic half-space was treated by Willis (1966), while more explicit expressions for a transversely isotropic half-space have been given, e.g., by Greszczuk (1982). Finite thickness increases the contact stiffness by reducing the surface displacement resulting from integration of strains. These effects were included in an approximate contact model by Suemasu et al. (1994). Large plate curvature ("wrapping") increases the contact stiffness by redistributing the contact stresses to a less concentrated load, which reduces the resulting indentation (e.g., Wu and Yen, 1994).

Small mass, wave controlled, impact response may be considered as a forced motion of an infinite plate. The forced motion of an infinite Kirchhoff plate was first treated by Boussinesq (1885) and was later considered in greater detail by Sneddon (1945). A solution for Hertzian impact on isotropic infinite Kirchhoff plates was presented by Zener (1941). Solutions for impact on orthotropic Kirchhoff plates were developed independently by Frischbier (1987) and Olsson (1989, 1992). A solution for impact on shear deformable quasi-isotropic plates was presented by Mittal (1987). This approach was later generalised by Olsson (2002) to orthotropic plates having either a Hertzian or a linear contact law, where the latter contact law is typical for sandwich panels. This paper also included explicit expressions for the numerical solution of the associated integral equations. A recent paper by Olsson (2003) used asymptotic cases to derive closed form approximations for the peak load during small mass impact on shear deformable plates.

The onset of delamination growth during impact on plates is obviously of great practical interest. A delamination growth criterion for static conditions was derived by Davies and Robinson (1992), who

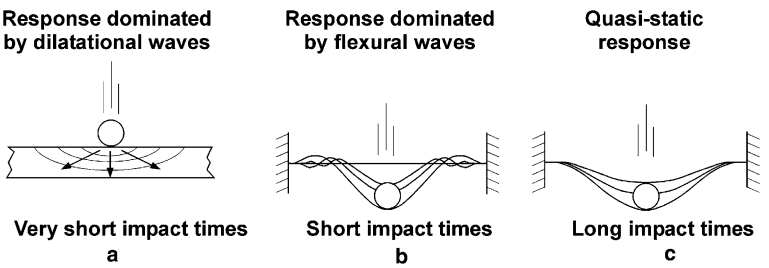

Fig. 1. Different response types during impact on plates.

showed that delamination growth occurs under a constant load independently of the delamination size. A different and more laborious approach was used by Suemasu and Majima (1996) who provided a more thorough derivation for an arbitrary number of delaminations. The effect of large deflections was considered in a later paper by Suemasu and Majima (1998). The small deflection perturbation approach used by Davies and Robinson (1992) implies that the delamination threshold load is independent of the boundary conditions of the plate, which has been demonstrated numerically by Olsson (2001). The delamination threshold load is supported by several experimental studies of quasi-static large mass impact for various laminates and boundary conditions (Davies and Robinson, 1992; Olsson, 2001; Cartié and Irving, 2002). A comparison with published experimental data indicated that the static delamination threshold load may also be relevant under truly dynamic conditions, i.e., during small mass impact (Olsson, 2003).

The present paper derives the delamination threshold load for small mass/high velocity impact on transversely isotropic plates, which often is a suitable homogenised approximation of laminates having many orthotropic plies equally and regularly distributed in at least three directions. It is shown that the inclusion of dynamic terms in the fracture mechanics criterion yields a delamination threshold load, which is somewhat larger than in the static case. The theoretical predictions are validated by comparison with explicit dynamic finite element simulations allowing initiation and growth of delaminations for a range of representative cases. Furthermore, a closed form approximation for the peak impact load is used to predict the corresponding threshold impact velocity. The predicted threshold velocities are compared with the FE simulations and published experimental results.

2. Closed form solutions

Consider a hemispherical impactor indenting a homogenous transversely isotropic elastic plate of thickness h at a contact load F. A first order approximation for the approach α between the impactor and the plate under small curvature was derived by Suemasu et al. (1994):

$$\begin{aligned} &\alpha = (F/k_{\mathrm{H}})^{2/3}\left(1 - \ln 2F^{1/3}k_{\mathrm{H}}^{2/3}K_0/h\right) \quad \text{where } \alpha \equiv w_{\mathrm{i}} - w_{\mathrm{p}} \\ &\text{or} \\ &\alpha = (F/k_{\mathrm{H}}^{*})^{2/3} \quad \text{where } k_{\mathrm{H}}^{*} = k_{\mathrm{H}}\Big/\left(1 - \ln 2F^{1/3}k_{\mathrm{H}}^{2/3}K_0/h\right)^{3/2}. \end{aligned} \tag{1}$$

Here w_{i} and w_{p} are the displacements of the impactor mass centre and the unloaded plate surface. The second form of Eq. (1), suggested here, recovers the Hertzian load-indentation relation assumed in the impact model described later and will be used in the following analysis.

For brevity, the complicated expression for the material constant K_0 is not repeated here. The contact stiffness k_{H} is given by the impactor tup radius R and the effective contact modulus Q_{H}:

$$k_{\mathrm{H}} = \tfrac{4}{3}Q_{\mathrm{H}}\sqrt{R} \quad \text{where } 1/Q_{\mathrm{H}} = 1/Q_{\mathrm{i}} + 1/Q_{\mathrm{p}} \tag{2}$$

and Q_{i} and Q_{p} are the effective contact moduli of the impactor and plate. Using earlier works Greszczuk (1982) derived the following expression for the contact modulus Q of a material with transverse isotropy along the loading axis z:

$$\begin{aligned} &Q = 2\sqrt{G_{rz}/C_{rr}}(C_{rr}C_{zz} - C_{rz}^2)\Big/\sqrt{\left(\sqrt{C_{rr}C_{zz}} + G_{zr}\right)^2 - \left(C_{rz} + G_{zr}\right)^2}, \\ &\text{where } C_{rr} = E_r(1 - v_{rz}v_{zr})\Omega/(1 + v_r), \quad C_{zz} = E_z(1 - v_r)\Omega, \\ &\qquad C_{rz} = E_r v_{zr}\Omega, \quad \Omega = 1/(1 - v_r - 2v_{rz}v_{zr}). \end{aligned} \tag{3}$$

The index r refers to the radial direction and the through-thickness Poisson's ratios are defined by $v_{rz} = \varepsilon_z/\varepsilon_r$ and $v_{zr} = \varepsilon_r/\varepsilon_z$ under uniaxial loading in the r- and z-direction, respectively.

Isotropic materials are special cases where the solution simplifies to

$$Q = E/(1 - v^2). \tag{4}$$

It should be noted that the tentative approximation $Q \approx E_z/(1 - v_{zr}v_{rz})$ suggested by Olsson (1992) underestimates the contact modulus of typical composite plates by 10–20%.

The contact stress distribution within the contact radius c is given by

$$p = p_0\sqrt{1 - r^2/c^2} \quad \text{where } p_0 = \tfrac{3}{2}F/\left(\pi c^2\right) \text{ and } c = \sqrt{R\alpha}. \tag{5}$$

Within plate theory the peak shear stress is given by $(3/2)\tau_{av}$, where the average shear stress τ_{av} is obtained by integrating Eq. (5) to obtain the surface load, and dividing by $2\pi hr$. The maximum shear stress $\tau_{\max}$ is found by differentiating the resulting expression with respect to the radius r:

$$\tau_{\max} = \tfrac{3}{2}F/(2\pi h r_1) \quad \text{where } r_1 = (3/4)^{1/4}c. \tag{6}$$

Combining Eqs. (1), (5) and (6) provides the corresponding threshold load F_τ for transverse matrix shear cracking. When finite thickness effects are neglected this load is given by

$$F_\tau = (4\pi/3)^{3/2}(\tau_U h)^{3/2}\sqrt{R/Q_{\mathrm{H}}}, \tag{7}$$

where τ_U is the out-of-plane shear strength of the plate.

The matrix shear cracks initiated at the shear threshold load, F_τ, gradually coalesce to form delaminations. A criterion for growth of these delaminations must be based on fracture mechanics. Within linear fracture mechanics the strain energy release rate G during dynamic fracture is given by (Hellan, 1985)

$$G = \mathrm{d}(W - U - T)/\mathrm{d}A, \tag{8}$$

where W is the work done by external forces, U is the strain energy, T is the kinetic energy associated with creation of the fracture area A. For a displacement w due to a single concentrated load, F, we obtain $W = 2U = Fw$ and the expression simplifies to

$$G = \mathrm{d}\left(\tfrac{1}{2}Fw - T\right)/\mathrm{d}A. \tag{9}$$

The description of the perturbation approach used by Davies and Robinson (1992) was very brief and limited to a single delamination. Furthermore, the applicability to general boundary conditions was not obvious. For these reasons the derivation of the static delamination threshold load will here be repeated for an arbitrary number of delaminations. For n delaminations the laminate will be divided into $n + 1$ sublaminates, with a total plate bending stiffness D_n given by

$$\begin{aligned} &D_n = (n+1)D/(n+1)^3 = D/(n+1)^2, \\ &\text{where } D = Q_{\mathrm{b}}h^3/12 \text{ and } Q_{\mathrm{b}} = E_r/(1 - v_r^2). \end{aligned} \tag{10}$$

Here v_r is the in-plane Poisson's ratio of the plate.

The shear stiffness S_n for the laminate with n delaminations is given by

$$S_n = (n+1)S/(n+1) = S, \quad \text{where } S = KG_{rz}h, \tag{11}$$

and K is the shear factor of the laminate, which for homogeneous plates is $K \approx 5/6$. Thus, shearing does not contribute to an increased deflection after delamination.

Consider the problem of a quasi-isotropic plate with arbitrary boundary conditions and a concentrated load acting in the centre of n circular delaminations of radius a (Fig. 2). The clamping of the delaminated region to the surrounding undelaminated region prevents sliding of the sublaminates. This implies that the

edge of the delaminated region remains plane and that the response to an applied edge moment is identical to that of an undelaminated plate, as long as no buckling occurs.

Within small deflection theory the additional deflection w caused by n delaminations is obtained by considering the deflections due to a central load on a circular plate with zero edge slope (i.e., clamped) after and before delamination, w_n and w_0, respectively. Thus

$$\frac{1}{2}Fw = \frac{1}{2}F(w_n - w_0) = \frac{1}{2}F\left(\frac{Fa^2}{16\pi D_n} - \frac{Fa^2}{16\pi D_0}\right) = \frac{F^2a^2}{32\pi D}\left[(n+1)^2 - 1\right] = \frac{F^2a^2}{32\pi D}n(n+2). \tag{12}$$

The delamination area of n delaminations with radius a is given by

$$\mathrm{d}A = 2n\pi a\,\mathrm{d}a. \tag{13}$$

For static conditions ($T = 0$) combining Eqs. (9), (12) and (13) yields,

$$G_{\mathrm{stat}} = \frac{(n+2)F^2}{32\pi^2 D}. \tag{14}$$

The equal deflection of all sublaminates implies a pure mode II loading. Thus the threshold load $F_{\mathrm{d}n}$ for growth of n delaminations under static conditions is given by

$$F_{\mathrm{d}n}^{\mathrm{stat}} = \pi\sqrt{32G_{\mathrm{IIc}}D/(n+2)}, \qquad F_{\mathrm{d}1}^{\mathrm{stat}} = \pi\sqrt{32G_{\mathrm{IIc}}D/3}, \tag{15}$$

where G_{IIc} is the critical strain energy release rate in mode II. In practice, delaminations form sequentially, with the first one appearing at the mid-plane where the shear stresses and resulting matrix cracks reach a maximum. Thus, the threshold load for *initiation* of delamination growth is given by $F_{\mathrm{d}1}$. Note that the delamination threshold load is *independent* of the delamination radius and therefore remains constant under static axisymmetric delamination growth with small deflections. This contrasts to the condition for delamination growth in centrally loaded beams, which is highly dependent on the delamination length (Davies and Robinson, 1992).

When neglecting transverse shear deformations, which are not affected by delamination, the deflection velocity immediately below a point load on a large plate (small mass impact) with n delaminations and mass per unit area m is given by (e.g., Mittal, 1987)

$$\dot{w}_n = \tfrac{1}{8}F/\sqrt{mD_n} = \tfrac{1}{8}(n+1)F/\sqrt{mD}. \tag{16}$$

The kinetic energy of a circular area with n delaminations is given by

$$T_n = \frac{1}{2}\int_0^a \dot{w}^2 m 2\pi r\,\mathrm{d}r = \pi m a^2 \dot{w}_n^2 \int_0^1 \bar{w}^2 s\,\mathrm{d}s = \frac{\pi}{64}\left[F^2a^2(n+1)^2/D\right]\frac{7}{108},$$
$$\text{where } s = r/a \text{ and } \bar{w} = (1 - s^2 + 2s^2\ln s). \tag{17}$$

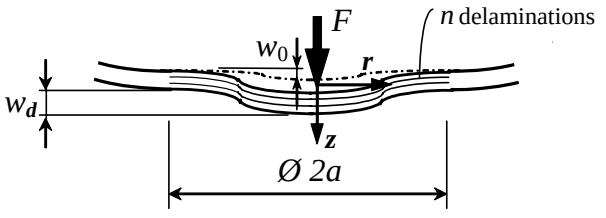

Fig. 2. Effect of delamination in large plate.

Here $\bar{w}$ is the normalised local deflection in a circular clamped plate under a central load. The value of the integral (7/108) was evaluated by somewhat lengthy but straightforward algebraic calculations. The kinetic energy T associated with forming n circular delaminations of radius a is obtained from the difference of the kinetic energy for the delaminated area after and before delamination, T_n and T_0, respectively:

$$T = T_n - T_0 = \frac{F^2 a^2}{32\pi D} n(n+2)\frac{7\pi^2}{216}. \tag{18}$$

For dynamic conditions ($T \neq 0$) combining Eqs. (9), (12), (13) and (18) yields

$$G_{\mathrm{dyn}} = G_{\mathrm{stat}}(1 - 7\pi^2/216), \tag{19}$$

where G_{stat} is given by Eq. (14).

The resulting delamination threshold load for small mass impact is given by

$$F_{\mathrm{d}n}^{\mathrm{dyn}} = F_{\mathrm{d}n}^{\mathrm{stat}} \Big/ \sqrt{1 - 7\pi^2/216} \approx 1.213 F_{\mathrm{d}n}^{\mathrm{stat}}, \tag{20}$$

where the static delamination threshold load $F_{\mathrm{d}n}^{\mathrm{stat}}$ is given by Eq. (15).

Interestingly, small mass impact conditions are predicted to cause a moderate increase in the threshold load for delamination growth, which is independent of the number and size of delaminations.

The ratio between the load for initiation of shear cracking and delamination is given by combining Eqs. (7), (15) and (20), which after simplification yields

$$F_\tau / F_{\mathrm{d1}}^{\mathrm{dyn}} = \tfrac{16}{9}\sqrt{(1 - 7\pi^2/216)2\pi/3}\ \tau_U^{3/2} \Big/ \sqrt{Q_{\mathrm{H}} Q_{\mathrm{b}} G_{\mathrm{IIc}}/R}, \tag{21}$$

where Q_{b} was defined in Eq. (10). It is found that most small mass impactors are predicted to cause shear cracking prior to delamination. For the application cases studied later in this article the load for initiation of shear failure is 36% of the delamination threshold load.

The criticality of an impact is easily assessed by comparing the predicted peak load under elastic conditions with the delamination threshold load $F_{\mathrm{d}n}^{\mathrm{dyn}}$. The peak impact load may either be predicted using a stepwise numerical solution of the appropriate integral equation (Olsson, 2002) or by using a closed form approximation based on asymptotic solutions (Olsson, 2003). The latter approach yields the following approximation for the peak impact load F_{peak} for a plate with Hertzian contact behaviour impacted by a mass M with a hemispherical tup:

$$\begin{aligned} &1/F_{\mathrm{peak}} \approx 1/F_{\mathrm{b}} + 1/F_{\mathrm{s}} + 1/F_{\mathrm{c}} \\ &\text{where } F_{\mathrm{b}} = 8V_0\sqrt{mD}, \quad F_{\mathrm{s}} = 2V_0\sqrt{\pi MS}, \quad F_{\mathrm{c}} = k_{\mathrm{H}}^{*2/5}\left(\tfrac{5}{4}MV_0^2\right)^{3/5}, \end{aligned} \tag{22}$$

where k_{H}^* from Eq. (1) is evaluated at the peak load.

The threshold velocity for delamination growth V_{d1} is obtained by equating the peak load F_{peak} with the delamination threshold load $F_{\mathrm{d1}}^{\mathrm{dyn}}$ and solving for V_0, which requires a brief iterative procedure.

The impact response history may be determined from a dimensionless integral equation, involving a normalised indentation and two dimensionless constants λ and β (Olsson, 2003):

$$\begin{aligned} &\lambda = M/\left(8T_{\mathrm{c}}\sqrt{mD}\right) = (4/5)^{3/5}F_{\mathrm{c}}/F_{\mathrm{b}}, \\ &\beta = \sqrt{mD}/(ST_{\mathrm{c}}) = \frac{\pi}{2}\lambda F_{\mathrm{b}}^2/F_{\mathrm{s}}^2 = \frac{\pi}{2}(4/5)^{3/5}F_{\mathrm{c}}F_{\mathrm{b}}/F_{\mathrm{s}}^2, \end{aligned} \tag{23}$$

where T_{c} is a time constant used for normalisation.

It is noted that λ is a measure of the relative flexural mobility of the plate, while β is a measure of the relative shear mobility. The elastic impact on a half-space is represented by $\lambda = \beta = 0$, which provides a symmetric impact load history with an impulse $2MV_0$ exerted to the plate. For increasing values of λ

the impact load history becomes increasingly asymmetric with a response dominated by plate flexure. For $\lambda > 2$ the impulse quickly approaches MV_0, which corresponds to an apparently inelastic impact. From Eq. (16) it may be concluded that the maximum deflection $w_n^{\max}$ of a Kirchhoff plate with n delaminations after completed impact at time t_{imp} is bound by

$$8\sqrt{mD}w_n^{\max}/(n+1) = \int_0^{t_{\text{imp}}} F(\tau)\,\mathrm{d}\tau \equiv I_{\max} \quad \text{where } MV_0 \leqslant I_{\max} \leqslant 2MV_0. \tag{24}$$

The properties of orthotropic plates may be represented by the following effective values (Olsson, 2003):

$$\begin{aligned} &D^* \approx \sqrt{D_{11}D_{22}}(\eta+1)/2 \\ &\text{where } \eta = (D_{12}+2D_{66})/\sqrt{D_{11}D_{22}}, \\ &\qquad S^* \approx \sqrt{A_{44}^* A_{55}^*} = \sqrt{K_{44}A_{44}K_{55}A_{55}}, \\ &\qquad v_{zr}^* v_{rz}^* \approx \sqrt{v_{zx}v_{xz}v_{zy}v_{yz}} = v_{xz}v_{yz}E_z/\sqrt{E_x E_y}, \end{aligned} \tag{25}$$

where K_{ij} are the shear factors and D_{ij} and A_{ij} are the bending and shear stiffness components given by laminated plate theory (Whitney, 1987). For Kirchhoff plates ($S^* = \infty$) use of D^* has been shown to yield a close approximation of the exact solution for the response (Olsson, 2003). Comparison with experimental data has also demonstrated the usefulness of this approximation for the quasi-static delamination threshold load in orthotropic plates (Olsson, 2001) and for estimating the delamination threshold load during dynamic small mass impact on laminates (Olsson, 2003). The errors associated with the approximation of the effective shear stiffness S^* should be moderate, as A_{44} and A_{55} usually are much more similar than D_{11} and D_{22}. The approximation of $v_{zr}^* v_{rz}^*$ should also have a small influence on the solution since this quantity is much less than unity.

3. Finite element validation

3.1. Finite element model

The finite element simulations were carried out using LS-DYNA (2003) explicit finite element code. The code formulation is based on the updated Lagrangian formulation which is used in conjunction with the central difference time integration scheme for integrating the resultant set of nonlinear dynamic equations. The method assumes a linear interpolation for velocities between two subsequent time steps and no stiffness matrix inversions are required during the analysis. The drawback of the explicit method used in LS-DYNA (2003) is that it is conditionally stable for nonlinear dynamic problems and the stability for its explicit operator is based on a critical value of the smallest time increment for a dilatational wave to cross any element in the mesh. Such a restriction can result in very small time step increments (in the order of nanoseconds for layered composites), depending on the degree of mesh refinement required in the analysis.

Finite element models of rectangular orthotropic plates were developed with thicknesses ranging from 2 to 6 mm. The dimensions of these plates were 102 mm by 152 mm, which is a common size of impact test specimens. The edges were assumed clamped and the hemispherical and rigid impactor had a mass of 3 g and a tup radius of 6 mm to simulate small mass/high velocity impact scenarios. Both impactor and plate were modelled using single-point integration solid elements available in LS-DYNA (2003). A sliding-line surface-to-surface contact logic, based on the penalty method formulation, was used to model the contact between the impactor and the plate. The material properties of the orthotropic plate are listed in Table 1. Central to the fidelity of the numerical model is the accurate representation of the initiation and possible propagation of delamination within the plate. Decohesion, or interface, elements were used for this purpose and these are described in more detail in Section 3.2.

Table 1
Material properties of the plate

$E_x = E_y = E_r$ [GPa]	E_z [GPa]	$G_{xz} = G_{yz} = G_{rz}$ [GPa]	$v_{xy} = v_r$ and $v_{yz} = v_{xz} = v_{rz}$	ρ [kg/m^3]
56.0	10.0	0.9, 4.5, 22.5	0.25	1600

The finite element mesh was generated using the mesh generator LS-INGRID by Stillman and Hallquist (1985). Interface elements were used to model the resin rich interface zone at the mid-plane of the plate, as shown in Fig. 3b. Using symmetry, only one-quarter of the plate was modelled and a typical FE mesh is shown in Fig. 3a. A finer mesh was assigned to the plate impact region in order to capture more accurately both initiation and delamination propagation during the impact simulations. A mesh sensitivity study was carried out for the 4 mm thick plate, using three different mesh densities for the plate impact region named coarse, medium and fine mesh. The meshes consisted of four by one, sixteen by two and thirty six by three elements per mm^3, respectively. Variations in the results for peak load and peak displacement values between coarse and medium meshes were less than 0.015% and around 0.01% between medium and fine meshes. In fact, this is not surprising since the interface element formulation is inherently meshing independent. Even though variations in results between coarse and fine meshes were negligible the fine mesh was used throughout the analysis to better represent the bending and through-thickness shear stress distributions. A viscous LS-DYNA hourglass control algorithm was used to avoid the formation of anomalous hourglass modes arising from reduced integration. The hourglass coefficient values were carefully chosen in order to minimise the energy dissipated by hourglass internal forces and its effects on the stable global deformation modes. As mentioned earlier, small mass impact responses are wave-dominated localised phenomena and therefore a relatively coarse mesh was used for regions far away from the impact region. In order to confirm such behaviour, the dimensions of the plate were doubled compared to the previous case and the plate was assumed to be unsupported. Both impact simulations presented identical responses and were unaffected by the boundary conditions over the time period in which damage initiation was observed.

3.2. Interface elements

Interface elements are decohesion elements, usually of zero thickness or of a finite thickness representing a resin-rich layer, which are inserted between composite layers or at well-defined interfaces where

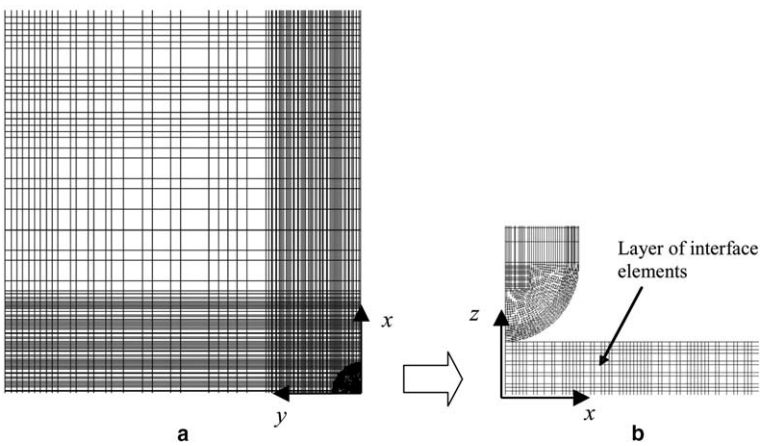

Fig. 3. Finite element model used for simulations: (a) Top view of the FE model and (b) interface layer at the mid-plane of the plate.

delamination is a possible failure mode. They provide a consistent means of simulating both stress-based initiation and energy-based propagation of delamination. They are also capable of representing mixed-mode delamination modelling without a priori knowledge of the mode ratio and are relatively mesh independent. The interface element formulation used in this study has a finite thickness of $t_{\text{int}} = 0.01$ mm and is based on the work proposed by Camanho and Davila (2002). It has been implemented into the LS-DYNA (2003) explicit finite element code as a material subroutine to be used with solid elements and has been experimentally validated by Pinho et al. (accepted for publication).

The interfacial constitutive law is defined in terms of a polynomial traction/relative displacements curve given by

$$\sigma_i = (27\sigma_i^0/4)[1 - 2(\delta_i/\delta_{fi}) + (\delta_i/\delta_{fi})^2](\delta_i/\delta_{fi}), \tag{26}$$

and shown in Fig. 4. σ_i^0 corresponds to the stress threshold at which damage initiates and δ_{f_i} is the critical displacement at which full decohesion occurs. The index i refers to either mode I, mode II or mode III. A linear elastic behaviour is assumed for mode I in compression to avoid interpenetration of the element. The failure displacement for each individual delamination mode is obtained from the integral of Eq. (26) which is equal to the fracture energy and is given by

$$G_{ic} = \int_0^{\delta_{f_i}} \sigma_i \, \mathrm{d}\delta_i = (27/48)\sigma_i^0 \delta_{f_i}. \tag{27}$$

For mixed-mode loading conditions the same constitutive law as given by Eq. (26) is assumed to hold for all modes and the stress threshold for each delamination mode is obtained from a quadratic stress-based criterion given by

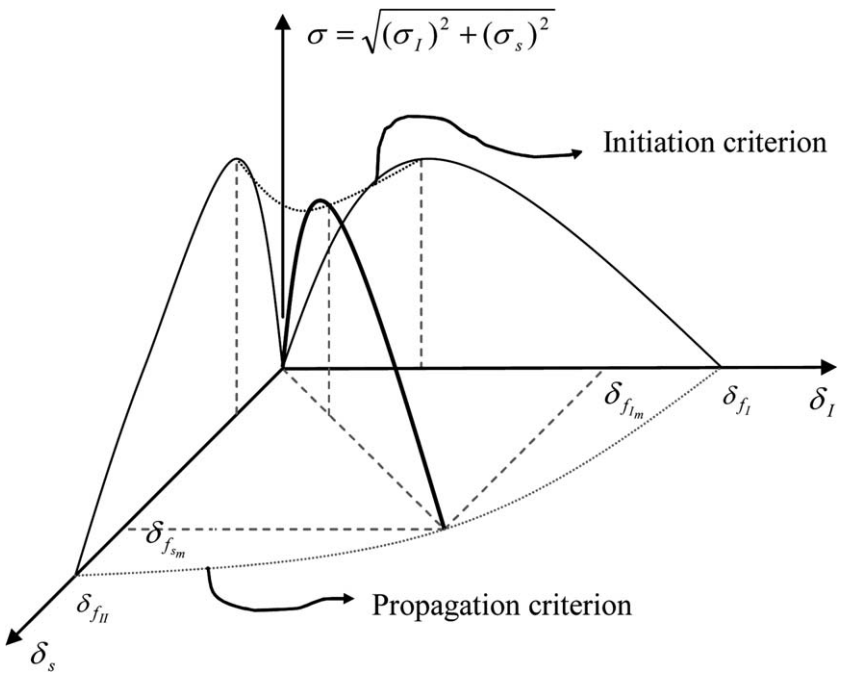

Fig. 4. Mixed-mode constitutive law for the interface element.

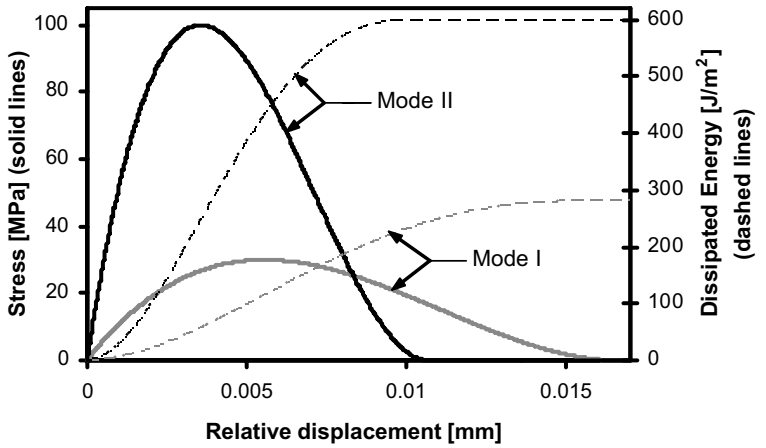

Fig. 5. Numerical stress-relative displacement curves for the interface element.

Table 2
Assumed strengths and interlaminar toughness properties

σ_n [MPa]	τ_U [MPa]	G_{Ic} [J/m^2]	G_{IIc} [J/m^2]	γ
30.0	100	281	600	1.0

$$\sigma^0_{I_m} = 1\Big/\sqrt{(1/\sigma_n)^2 + (\xi/\tau_U)^2}, \tag{28}$$

$$\sigma^0_{s_m} = \xi\sigma^0_{I_m}, \tag{29}$$

where the subscripts s and I refer to the resultant shear stress and normal tensile stress, respectively; m refers to mixed-mode loading conditions and σ_n and τ_U are the normal and transverse interlaminar shear strengths, respectively.

The interface constitutive law for mixed-mode loading conditions is illustrated in Fig. 5. ξ is defined as the mode ratio parameter, which is the ratio between normal mode I and the resultant mode II/III shear displacements. The determination of the failure displacements is based on a power law propagation criterion, considering the stresses defined in Eqs. (28) and (29) and the critical strain energy release rates in modes I and II, G_{Ic} and G_{IIc}, respectively:

$$\delta_{f_{I_m}} = (48/27)\left[(\sigma^0_{I_m}/G_{\mathrm{Ic}})^\gamma + (\sigma^0_{s_m}/G_{\mathrm{IIc}})^\gamma\right]^{-1/\gamma}, \tag{30}$$

$$\delta_{f_{s_m}} = \xi\delta_{f_{I_m}}. \tag{31}$$

The interface parameters used in this study are given in Table 2.

4. Parametric study

The accuracy of the theory was studied by comparison with finite element simulations for a range of representative cases. The impactor was assumed to be rigid with 6 mm tup radius and a mass of 3 g, which is representative of a small piece of runway debris. The assumption of a rigid impactor was done to simplify the finite element modelling, but this assumption is by no means required in any of the models or equations described in this paper.

Table 3
Overview of cases studied

Thickness, h [mm]	2	3	4	5	6	4	4
Shear modulus, G_{rz} [GPa]	4.5	4.5	4.5	4.5	4.5	0.9	22.5
Flexural mobility, λ	2.89	1.31	0.76	0.50	0.36	0.61	0.88
Shear mobility, β	0.13	0.20	0.27	0.35	0.44	1.10	0.06

The material properties of the plate were selected to be representative of a homogenised quasi-isotropic laminate of a typical carbon/epoxy composite. Table 1 listed the assumed density and elastic properties. Table 2 listed the out-of-plane tensile strength σ_n and shear strength τ_U and the critical strain energy release rates in mode I, G_{Ic}, and mode II, G_{IIc}. A linear interaction ($\gamma = 1$) was assumed for the delamination propagation criterion, Eq. (30).

The influence of increasing relative bending stiffness was studied for plate thicknesses between 2 and 6 mm, which are common in the outer parts of an aircraft wing. Most of the simulations assumed a through-thickness shear modulus of 4.5 GPa, which is typical for a carbon/epoxy laminate. However, to study the influence of changes in the shear stiffness, the response of the 4 mm plate was also examined for an isotropic E_r/G_{rz} ratio ($G_{rz} = 22.5$ GPa) and for a plate with very low shear modulus ($G_{rz} = 0.9$ GPa). An overview of the different cases is given in Table 3, which shows that the test matrix ranges from cases dominated by indentation ($\lambda \approx 0$) to cases dominated by plate bending ($\lambda > 2$). The relative shear mobility is typical for impact on composite laminates, but also covers two extreme cases where $\beta \approx 0$ and $\beta > 1$.

For each case the delamination threshold load and threshold velocity were found by successively increasing the impactor velocity in steps of 0.5 m/s until delamination occurred.

5. Experimental comparisons

To demonstrate the ability to predict delamination onset in real laminates the theoretical predictions were compared with published experimental results. Load measurement during small-mass high-velocity impact is difficult to perform and published experimental results are scarce. Furthermore, the finite size and stiffness of real impactors produce superimposed stress waves, which effectively prevent detection of delamination onset from the load history. An example of a load history may be found in Olsson (2000). For these reasons comparisons were limited to experimental observations of the delamination threshold velocity. Several experimental threshold velocities are based on fairly crude extrapolation, since most experiments were not focused on finding delamination thresholds.

The comparisons are shown in Table 4, which was originally presented in Olsson (2003) but has been updated to account for the current dynamic delamination threshold load and the improved contact theory used in the present article. The comparisons in Olsson (2003) also included a 0.5 mm laminate which has been excluded from the present comparison, as the predicted deflection at peak load grossly exceeds the range of validity of the current small deflection theory. The first four laminates are transversely isotropic (“quasi-isotropic”). The properties of the remaining four orthotropic laminates were estimated using the effective properties suggested in Eq. (25). Further details on the assumed material properties may be found in Olsson (2003). The apparent contact modulus Q_{H}^{*} accounts for the corrected Q_{H} resulting from the out-of-plane stiffness of the plate given in Eq. (3) and the finite thickness enhancement $k_{\mathrm{H}}^{*}/k_{\mathrm{H}}$ given by Eq. (1). For the material AS4/PEEK two different values of G_{IIc} have been given. The higher value is based on typical published values discussed by Olsson (2003). The lower value was deduced from accompanying large mass (quasi-static) impact tests by Morita et al. (1997), using the quasi-static model for damage onset in Olsson (2001).

Table 4
Predicted and observed delamination threshold velocities

Plate material	Layup	h [mm]	Q_H^* [a] [GPa]	Q_f^* [b] [GPa]	G_{rz}^* [c] [GPa]	G_{IIc} [J/m^2]	Impactor material	R [mm]	M [g]	V_{pred} [m/s]	V_{exp} [m/s]	Ref.
HTA/6376C	$[(0/\pm45/90)_s/(90/\mp45/0)_s]_3$	6.2	12	54	4.3	600	Aluminium	11	10.2	32	28	Olsson (2003)
AS4/PEEK	$(0_3/45_3/90_3/-45_3)_s$	3.2	12	59	4.4	1959[d]	Aluminium	6.4	1.9	68	46	Morita et al. (1997)
AS4/PEEK	$(0_3/45_3/90_3/-45_3)_s$	3.2	12	59	4.4	950[e]	Aluminium	6.4	1.9	49	46	Morita et al. (1997)
T300/5208	$(0/\pm45/90)_{6s}$	6.2	12	57	5.0	300	Aluminium	6.4	3.0	38	38	Williams (1984)
AS4/2220-3	$(0/\pm45/90)_{6s}$	6.2	13	54	6.0	510	Aluminium	6.4	3.0	46	55	Williams (1984)
AS4/3501-6	$(0_2/90_2)_7/0_2$	3.8	∞	55	4.8	600	Steel	∞	14.6	21	17[f]	Malvern et al. (1989)
XAS/914C	$[0_2/\pm45]_{2s}$	2.0	12	48	4.6	416	Steel	3	0.9	34	30	Cantwell and Morton (1989)
XAS/914C	$[0/90]_{8s}$	4.0	12	57	4.6	416	Steel	3	0.9	54	47[f]	Cantwell (1988)
XAS/914C	$[0/90]_{2s}$	1.0	13	54	4.6	416	Steel	3	0.9	32	33	Cantwell (1988)

[a] $Q_H^* = Q_H k_H^*/k_H$.
[b] $Q_f^* = 12D^*/h^3$.
[c] $G_{rz}^* = (A_{44}A_{55})^{1/2}/h$.
[d] Nominal toughness.
[e] Deduced from quasi-static impact tests in Morita et al. (1997).
[f] Extrapolated from 30% to 50% higher velocity.

6. Results and discussion

An example of the finite element simulations is given in Fig. 6, which shows the response of the 4 mm plate with $G_{rz} = 4.5$ GPa at the delamination threshold velocity. Common features of all cases were an asymmetric load history and a deflection essentially proportional to the load-time integral, i.e., the impulse.

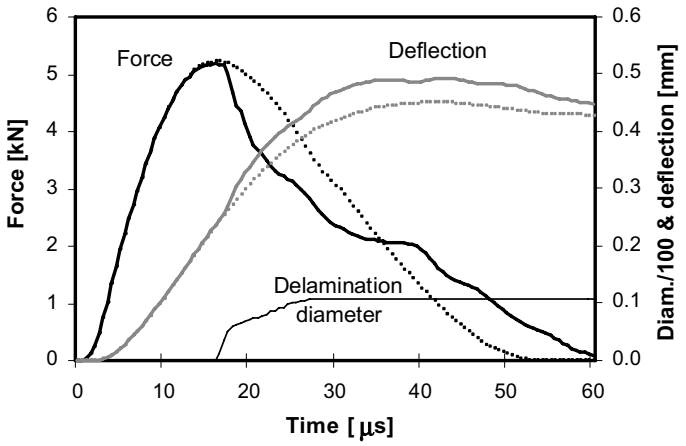

Fig. 6. Finite element simulation of response history for 4 mm plate with $G_{rz} = 4.5$ GPa (dashed curve = no delamination, solid curve = with delamination).

The response without delamination is in agreement with previous experimental results and theoretical predictions, e.g., Olsson (1992).

The theoretical assumption of pure mode II delamination growth was fully confirmed by the finite element results. The onset of delamination occurs at the peak load and causes a rapidly decreasing load, accompanied by a quasi-unstable delamination growth until a certain size is reached (Fig. 6). Thus, the delamination size shows a step increase at the delamination threshold velocity. Furthermore, in contrast to the quasi-static growth during large mass impacts, the delamination growth does not occur under constant load. The delamination onset causes a sudden but temporary increase in the deflection velocity (Fig. 7), while the influence on maximum plate deflection is fairly small (Fig. 6). The deflection history of the shear compliant plate was significantly different, with a very limited effect of the delamination onset at 22 μs (Fig. 8).

The delamination threshold load obtained in the finite element simulation is in very good agreement with the theoretical predictions (Figs. 9 and 10). This validates that the theoretical threshold load may be used as a criterion for delamination onset during small mass/high velocity impact.

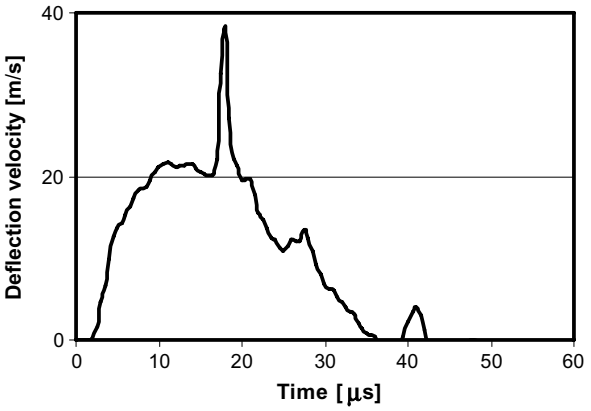

Fig. 7. Finite element simulation of deflection velocity for 4 mm plate with $G_{rz} = 4.5$ GPa.

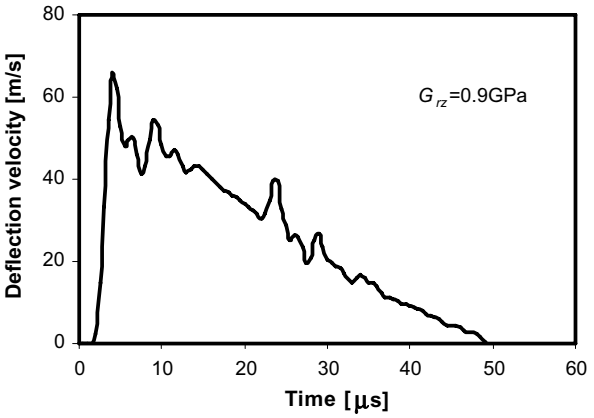

Fig. 8. Finite element simulation of deflection velocity for 4 mm plate with G_{rz}=0.9 GPa.

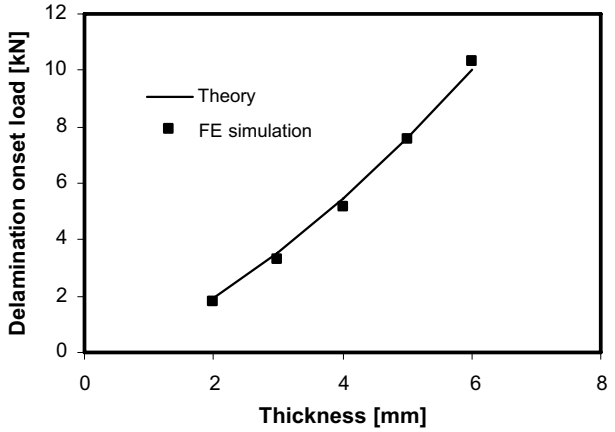

Fig. 9. Predicted delamination threshold loads for plates with $G_{rz} = 4.5$ GPa.

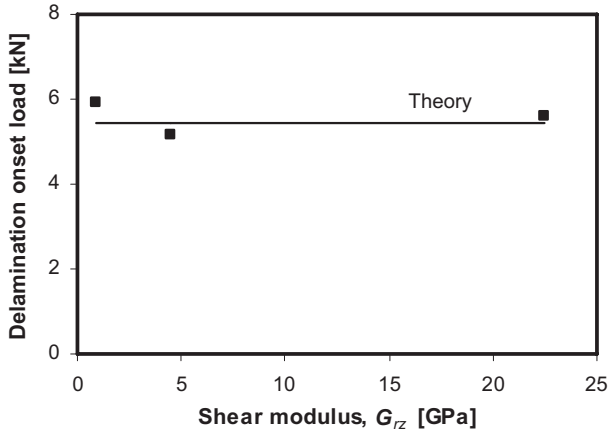

Fig. 10. Predicted delamination threshold loads for 4 mm thick plates.

There is also a good agreement between the change in plate deflection velocity obtained in the finite element simulation and the theory, Eq. (16), which predicts a doubled deflection velocity immediately after formation of a single delamination (Fig. 11). Interestingly, the finite element simulations demonstrate that the delamination causes a spike in the deflection velocity, which then appears to return to its original value (Fig. 7). The only exception of this behaviour was the plate with low shear stiffness ($G_{rz} = 0.9$ GPa), where the deflection velocity history was only slightly influenced by the delamination event (Fig. 8). The small number of time steps during the spike does not, however, allow a very accurate computation of the deflection velocity transient. A refined FE-mesh for the baseline 4 mm plate did, for example, increase the deflection velocity rate from 1.91 to 2.05. Thus, the variations in Fig. 11 are more likely to reflect a moderate computational accuracy than an actual influence of plate thickness.

The theoretically predicted delamination threshold velocities using Eq. (22) for a fixed mass of 3 g are also in good agreement with the finite element simulations (Figs. 12 and 13). The theoretical model underestimates the threshold velocity when the shear modulus is very low, which indicates that it does not fully

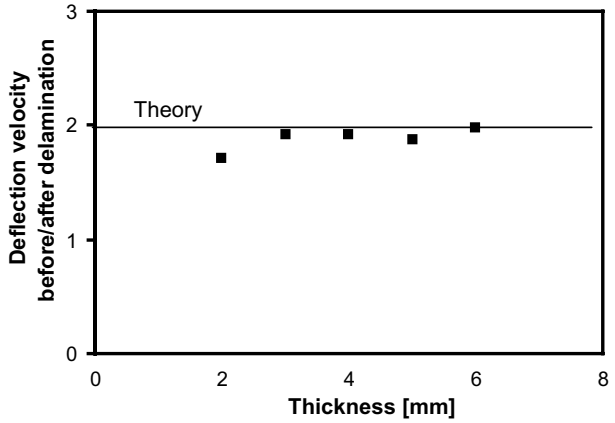

Fig. 11. Predicted change in deflection velocity for plates with $G_{rz} = 4.5$ GPa.

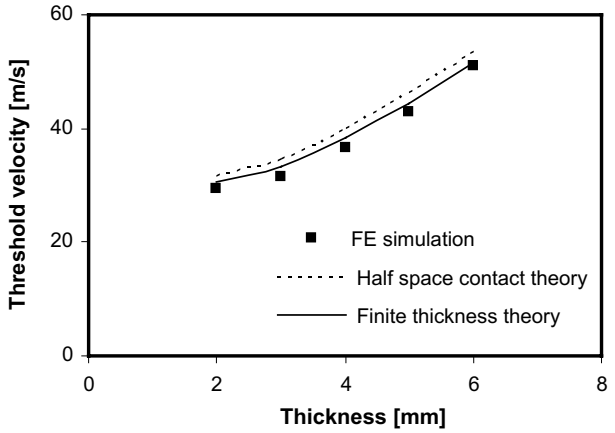

Fig. 12. Predicted delamination threshold velocities for plates with $G_{rz} = 4.5$ GPa.

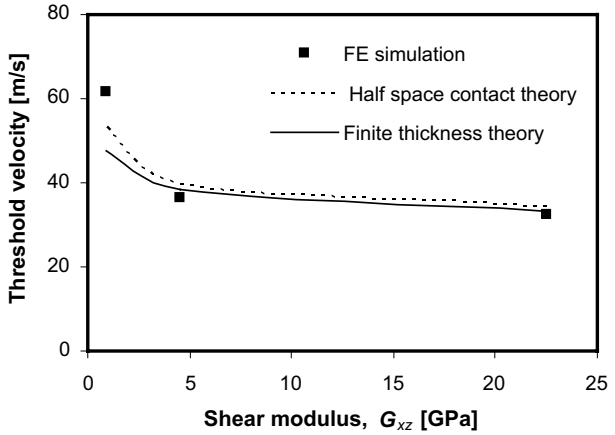

Fig. 13. Predicted delamination threshold velocities for 4 mm thick plates.

account for shear deformations (Fig. 13). The finite thickness contact theory for the highest shear modulus was based on an apparent asymptotic value of $K_0 = 2 \times 10^{-11}$ m^2/N in Eq. (1), as the expressions for K_0 given by Suemasu et al. (1994) were undefined for $G_{rz} = 22.5$ GPa. It is noted that the neglect of finite thickness results in a slight overestimation of the threshold velocity. An additional overestimation of the same order would be obtained by approximating the modulus by $Q_p = E_z/(1 - v_{rz}v_{zr}) \approx E_z$, which increases the indentation by 16%.

Fig. 14 gives a comparison between the theoretically predicted contact radius and the indentations predicted by theory and finite element analysis. This graph demonstrates that the error due to neglect of finite thickness decreases with decreasing contact radius, as expected, but that the finite thickness effect remains evident for all cases studied.

With a few exceptions there is a good agreement between predicted and experimentally observed delamination threshold velocities (Table 4). The agreement for the AS4/PEEK laminate is poor when using a typical value of G_{IIc} but good when using the low toughness deduced from the delamination onset in accompanying quasi-static drop weight tests. It is well known that the toughness of AS4/PEEK (APC2) could be halved by a high crystallinity after too slow cooling during manufacturing (Talbott et al., 1987). These specimens were indeed manufactured with a slow cooling rate of 2 °C/min down to 320 °C followed by 10 °C/min to room temperature (Adachi, T., 2005. Personal communication, Tokyo Institute of Technology). There is no significant difference in the experimental agreement for the quasi-isotropic and orthotropic laminates, which indicates that the effective properties in Eq. (25) can be used to estimate the delamination threshold load of orthotropic laminates. Further theoretical work is, however, required to validate this conclusion.

The present theory does not account for membrane effects due to large deflections. Such effects are normally less important during small mass impact, as the peak deflection generally is smaller than in large mass impact. Furthermore, delamination onset occurs at the peak load, when the deflection is significantly smaller than the expected peak deflection (after completed impact). In fact, the deflection at delamination onset was a fraction of the plate deflection for all cases considered in the parametric study as well as in the experimental comparison.

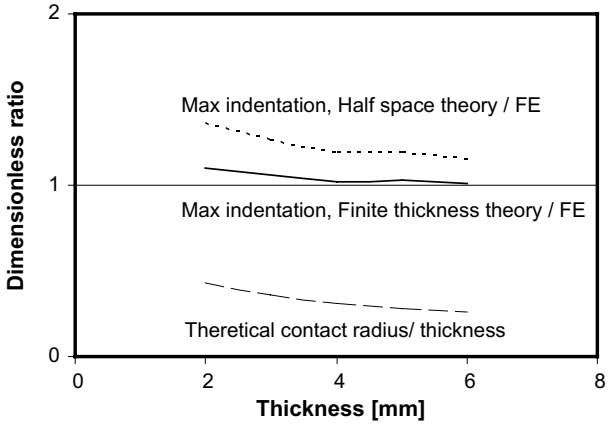

Fig. 14. Predicted indentation and contact radius for plates with $G_{rz} = 4.5$ GPa.

7. Conclusions

The presented closed form solution for predicting the onset of delamination in a transversely isotropic laminated plate under small mass/high velocity impact was validated against detailed finite element models of plates with different thickness. This validation was predominantly based on comparing the impactor force and the change in deflection velocities resulting from the onset of mid-plane delamination for different shear stiffness. Very good agreement was achieved for the plate thicknesses investigated, ranging from 2 to 6 mm. This shows that the presently derived delamination threshold load should be useful as a criterion for delamination onset in theoretical and numerical models of impact.

Theoretical predictions of the delamination threshold velocity were obtained by combining the delamination threshold load with an available solution for prediction of peak load during impact. The predictions were in good agreement with the finite element simulations. Slightly better correlation was demonstrated by including the finite thickness effects in the contact analysis. The threshold velocity was under-predicted for very low transverse shear stiffness, indicating that higher order shear deformation needs to be accounted for in such instances. It may be concluded that the suggested approach can be used for closed form prediction of delamination threshold velocities in experiments and design applications.

With a few exceptions the predicted delamination threshold velocities also showed good agreement with published experimental results for quasi-isotropic and orthotropic laminates made of various fibre/polymer composites.

The present study was focused on the onset of delamination growth at the most critical interface. Future studies should consider the subsequent initiation and growth of delaminations at multiple interfaces. A further issue of interest is delamination growth in homogeneous orthotropic plates and in laminated plates with orthotropic plies of different orientation.

Acknowledgements

The authors are indebted to Dr. P. Robinson for explaining some issues regarding the static delamination growth model suggested by Davies and Robinson (1992). They are also grateful to the Brazilian National Research Council (CNPq) for the financial support received for the computational part of this work through the contract number 200863/00-2.

References

Abrate, S., 1991. Impact on laminated composite materials. Applied Mechanics Reviews 44 (4), 155–190.

Boussinesq, J.N., 1885. Application Des Potentiels à L'étude De L'équilibre Et Du Movement Des Solides élastiques. Gauthier-Villars, Paris, pp. 464–480.

Camanho, P.P., Davila, C.G., 2002. Mixed-mode decohesion finite elements for the simulation of delamination in composite materials, NASA/TM-2002-211737.

Cantwell, W.J., 1988. The influence of target geometry on the high velocity impact response of CFRP. Composite Structures 10 (3), 247–265.

Cantwell, W.J., Morton, J., 1989. Comparison of the low and high velocity impact response of CFRP. Composites 20 (6), 545–551.

Cartié, D.D.R., Irving, P.E., 2002. Effect of resin and fibre properties on impact and compression after impact of CFRP. Composites Part A 33 (4), 483–493.

Davies, G.A.O., Olsson, R., 2004. Impact on composite structures. The Aeronautical Journal 108 (1089), 541–563.

Davies, G.A.O., Robinson, P., 1992. Predicting failure by debonding/delamination. In: Debonding/Delamination of Composites, AGARD Conf. Proc. 530. AGARD, Neuilly sur Seine, France.

Frischbier, J., 1987. Theorie der Stossbelastung orthotroper Platten und ihre experimentelle Überprüfung, Mitteilung Nr. 51. Institut für Mechanik, Rühr-Universität, Bochum, Germany.

Greszczuk, L.B., 1982. Damage in composite materials due to low velocity impact. In: Zukas, J.A. et al. (Eds.), Impact Dynamics. John Wiley & Sons, New York, pp. 55–94.

Hellan, K., 1985. Introduction to Fracture Mechanics. McGraw-Hill, New York.

LS-DYNA 970, 2003. Livermore Software Technology Corporation, USA.

Malvern, L.E., Sun, C.T., Liu, D., 1989. Delamination damage in central impacts at subperforation speeds on laminated kevlar/epoxy laminates. In: Composite Materials: Fatigue and FractureASTM STP 1012, vol. 2. ASTM, Philadelphia, pp. 387–405.

Mittal, R.K., 1987. A simplified analysis of the effect of transverse shear on the response of elastic plates to impact loading. International Journal of Solids and Structures 23 (8), 1191–1203.

Morita, H., Adachi, T., Tateishi, Y., Matsumoto, H., 1997. Characterization of impact damage resistance of CF/PEEK and CF/toughened epoxy laminates under low and high velocity impact tests. Journal of Reinforced Plastics and Composites 16 (2), 131–143.

Olsson, R., 1989. Impact response of orthotropic composite plates predicted by a one-parameter differential equation, FFA TN 1989-07. The Aeron. Res. Inst. of Sweden, Bromma, Sweden.

Olsson, R., 1992. Impact response of orthotropic composite laminates predicted from a one-parameter differential equation. AIAA Journal 30 (6), 1587–1596.

Olsson, R., 2000. Mass criterion for wave controlled impact response of composite plates. Composites Part A 31 (8), 879–887, Correction in Composites Part A 32 (2), 291.

Olsson, R., 2001. Analytical prediction of large mass impact damage in composite laminates. Composites Part A 32 (9), 1207–1215.

Olsson, R., 2002. Engineering method for prediction of impact response and damage in sandwich panels. Journal of Sandwich Structures and Materials 4 (1), 83–95.

Olsson, R., 2003. Closed form prediction of peak load and delamination onset under small mass impact. Composite Structures 59 (3), 340–348.

Pinho, S.T., Iannucci, L., Robinson, P., accepted for publication. Formulation and implementation of decohesion elements in an explicit finite element code. Composites: Part A.

Sneddon, I.N., 1945. The symmetrical vibrations of a thin elastic plate. Proceedings of Cambridge Philosophical Society 41 (1), 27–43.

Stillman, D.W., Hallquist, J.O., 1985. LS-INGRID: A Three-dimensional Mesh Generator for Modelling Non-Linear Systems. University of California, Lawrence Livermore National Laboratory, USA.

Suemasu, H., Majima, O., 1996. Multiple delaminations and their severity in circular axisymmetric plates subjected to transverse loading. Journal of Composite Materials 30 (4), 441–453.

Suemasu, H., Majima, O., 1998. Multiple delaminations and their severity in nonlinear circular plates subjected to concentrated loading. Journal of Composite Materials 32 (2), 123–140.

Suemasu, H., Kerth, S., Maier, M., 1994. Indentation of spherical head indentors on transversely isotropic composite plates. Journal of Composite Materials 28 (17), 1723–1739.

Talbott, M.F., Springer, G.S., Berglund, L.A., 1987. The effects of crystallinity on the mechanical properties of PEEK polymer and graphite fiber reinforced PEEK. Journal of Composite Materials 21 (11), 1056–1081.

Whitney, J.M., 1987. Structural Analysis of Laminated Anisotropic Plates. Technomic, Lancaster, PA.

Williams, J.G., 1984. Effect of impact damage and open holes on the compression strength of tough resin/high strain fiber laminates. Tough composite materials. NASA CP 2334. pp. 61–79.

Willis, J.R., 1966. Hertzian contact of anisotropic bodies. Journal of the Mechanics and Physics of Solids 14 (3), 163–176.

Wu, E., Yen, C.S., 1994. The contact behaviour between laminated composite plates and rigid spheres. Transactions of ASME, Journal of Applied Mechanics 61 (1), 60–66.

Zener, C., 1941. The intrinsic inelasticity of large plates. Physical Review 59, 669–673.